Top Curr Chem
DOI 10.1007/128_2007_28

Microcantilever Sensors

Hans Peter Lang (✉) · Christoph Gerber (✉)

National Competence Center for Research in Nanoscale Science, University of Basel, Institute of Physics, Klingelbergstrasse 82, 4056 Basel, Switzerland
Hans-Peter.Lang@unibas.ch, Christoph.Gerber@unibas.ch

Abstract Microfabricated cantilevers have been used in atomic force microscopy for the topography imaging of non-conductive surfaces for more than 20 years. Cantilever beams without tips have proved their applicability in recent years as miniaturized, ultrasensitive, and fast-responding sensors for applications in chemistry, physics, biochemistry, and medicine. Microcantilever sensors respond by bending due to the absorption of molecules. A shift in resonance frequency also occurs. They can be operated in different environments such as gaseous environment, liquids, or vacuum. In gas, microcantilever sensors can be operated as an artificial nose, whereby the bending pattern of a microfabricated array of eight polymer-coated silicon cantilevers is characteristic of the different vapors from solvents, flavors, and beverages. When operated in a liquid, microcantilever sensors are able to detect biochemical reactions. Each cantilever is functionalized with a specific biochemical probe receptor, sensitive for detection of the corresponding target molecule. Applications lie in the fields of label- and amplification-free detection of

DNA hybridization, the detection of proteins as well as antigen-antibody reactions, and the detection of larger entities, such as bacteria and fungi.

Keywords Artificial nose · Biosensor · Microcantilever sensor

Abbreviations

AFM	Atomic force microscopy
CMC	Carboxymethyl cellulose
CMOS	Complementary metal oxide semiconductor
DDT	Dichlorodiphenyltrichloroethane
DIMP	Diisopropyl methyl phosphonate
DMMP	Dimethylmethylphosphonate
DNA	Deoxyribonucleic acid
DNT	Dinitrotoluene
HPC	Hydroxypropyl cellulose
HPLC	High Performance Liquid Chromatography
PAAM	Poly(allylamine)
PC	Personal computer
PCA	Principal component analysis
PEEK	Poly-etheretherketone
PEI	Polyethylenimine
PEO	Poly(2-ethyl-2-oxazoline)
PETN	Pentaerythritol tetranitrate
PSA	Prostate-specific antigen
PSD	Position sensitive detector
PSS	Polystyrenesulfonate
PVP	Polyvinylpyrrolidone
PZT	Lead zirconium titanate
RDX	Hexahydro-1,3,5-triazine
QCM	Quarz crystal microbalance
SPR	Surface plasmon resonance
TNT	Trinitrotoluene
VCSEL	Vertical cavity surface emitting laser
VOC	Volatile organic compound

1 Introduction to Microcantilever Sensors

1.1 Historical Development

Measurement of adsorption-induced bending or a change in resonance frequency using beams of silicon as sensors was already described in literature in 1968, by Wilfinger et al. [1], who detected resonances in large silicon cantilever structures of 50 mm × 30 mm × 8 mm. Actuation was realized by localized thermal expansion in diffused resistors (piezoresistors) located near

the cantilever support to create a temperature gradient for driving the cantilever at its resonance frequency. Similarly, the piezoresistors could also be used to monitor mechanical deflection of the cantilever. Heng [2] fabricated in 1971 gold microcantilevers capacitively coupled to microstrip lines for the mechanical trimming of high-frequency oscillator circuits. Petersen [3] constructed in 1979 cantilever-type micromechanical membrane switches made from silicon designed to bridge the gap between silicon transistors and mechanical electromagnetic relays. Kolesar [4] suggested in 1985 the use of cantilever structures as electronic detectors for nerve agents.

Since the advent of atomic force microscopy (AFM) in 1986 [5] microfabricated cantilevers have become easily commercially available, triggering research reports on the use of microcantilevers as sensors. In 1994, Itoh et al. [6] presented a microcantilever coated with a thin film of zinc-oxide with piezoresistive deflection readout. Cleveland et al. [7] reported the tracking of cantilever resonance frequency to detect nanogram changes in mass loading when small particles are deposited onto AFM probe tips. Gimzewski et al. [8] showed the first chemical sensing applications, in which static cantilever bending revealed chemical reactions, such as the platinum-assisted catalytic conversion of hydrogen and oxygen into water at very high sensitivity. Thundat et al. [9] demonstrated that the resonance frequency as well as the static bending of microcantilevers is influenced by changing ambient conditions, such as moisture adsorption. Furthermore, they found that the deflection of metal-coated cantilevers is also thermally influenced (the bimetallic effect). Later, Thundat et al. [10] observed changes in the resonance frequency of microcantilevers due to the adsorption of analyte vapor on exposed surfaces. The frequency changes are due to mass loading or adsorption-induced changes in the cantilever spring constant. By coating cantilever surfaces with hygroscopic materials, such as phosphoric acid or gelatin, the cantilever can sense water vapor at picogram mass resolution.

1.2 Measurement Principle

1.2.1 Concept

Microcantilevers as sensors, unlike AFM cantilevers, neither need a tip at their apex nor a sample surface. The microcantilever surfaces serve as sensors, in particular, to detect the adsorption of molecules taking place on these surfaces. The generation of surface stress is monitored, eventually resulting in the bending of the microcantilever, if the adsorption preferentially occurs on one of its surfaces. Selective adsorption is controlled by coating one surface (typically the upper surface) of a microcantilever with a thin layer of a material that shows an affinity to molecules in the environment (sensor surface).

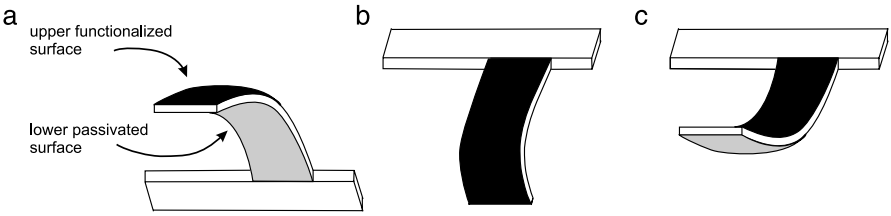

Fig. 1 **a** Schematic drawing of a microcantilever with its lower surface passivated and it upper surface functionalized for recognition of target molecules, **b** downward bending of a microcantilever due to compressive surface stress, **c** upward bending due to tensile surface stress

We call this surface the "functionalized" surface of the microcantilever (see Fig. 1a). The other surface of the cantilever (typically the lower surface) may be left uncoated or can be coated with a passivation layer, which is either inert or does not exhibit significant affinity to the molecules in the environment to be detected. To establish functionalized surfaces, often a metal layer is evaporated onto the surface designed as a sensor surface. Metal surfaces, such as gold, may be used to covalently bind a monolayer constituting the chemical surface sensitive to the molecules to be detected. Often, a monolayer of thiol molecules, offering defined surface chemistry, is covalently bound to a gold surface. The gold layer also serves as a reflection layer if the bending of the cantilever is read out optically.

1.2.2
Compressive and Tensile Stress

Adsorption of molecules on the upper (functionalized) surface will result in a downward bending of the microcantilever due to the formation of surface stress. We will call the surface stress "compressive" (see Fig. 1b), because the adsorbed layer of molecules (e.g., a monolayer of alkylthiols) produces a downward bending of the microcantilever away from its functionalized side. If the opposite situation occurs, i.e., when the microcantilever bends upwards, we would speak of "tensile stress" (see Fig. 1c). If both the upper and the lower surface of the microcantilever are exposed to surface stress changes, then the situation will be much more complex, as a predominant compressive stress formation on the lower microcantilever surface might appear as tensile stress on the upper surface. For this reason, it is extremely important to properly passivate the lower surface so that, ideally, no processes take place on the lower surface of the microcantilever. Various strategies can be used to passivate the lower surface of microcantilevers. For biochemical systems, the application of a thin layer of 2-[methoxy-poly(ethyleneoxy)propyl]trimethoxysilane will create a pegylated surface that is almost inert towards the adsorption of biological layers. For the detection of gases, coating with a gold layer will passivate the sur-

face. For the recognition of solvent vapors, coating with a fluorinated polymer layer will serve as a non-reactive layer. The actual experiment will show whether the passivation layer was really efficient, as such passivated cantilevers will not show a substantial bending response upon exposure to an analyte.

1.2.3 Differential Measurements

Single microcantilevers may bend due to thermal drift or an interaction with their environment, in particular if operated in a liquid. Furthermore, nonspecific physisorption of molecules on the cantilever surface or nonspecific binding to receptor molecules during measurements may contribute to the drift.

To exclude such influences, the simultaneous measurement of reference microcantilevers aligned in the same array as the sensing microcantilevers is crucial [11]. The difference in signals from the reference and sensor microcantilevers yields the net bending response, and even small sensor signals can be extracted from large microcantilever deflections without being dominated by undesired effects. When only single microcantilevers are used, no thermal-drift compensation is possible. To obtain useful data under these circumstances, both microcantilever surfaces have to be chemically well-defined. One of the surfaces, typically the lower one, has to be passivated; otherwise, the microcantilever response will be convoluted with undesired effects originating from uncontrolled reactions taking place on the lower surface. With a pair of microcantilevers, reliable measurements are obtained. One of them is used as the sensor microcantilever (coated typically on the upper side with a molecule layer that shows affinity to the molecules to be detected), whereas the other microcantilever serves as the reference. It should be coated with a passivation layer on the upper surface so as not to exhibit affinity to the molecules to be detected. Thermal drifts are cancelled out if difference responses, i.e., the difference in deflections of sensor and reference microcantilevers are taken (differential measurements). Alternatively, both microcantilevers are used as sensors (sensor layers on the upper surfaces), and the lower surface has to be passivated. It is best to use an array of microcantilevers, in which some are used either as sensor or as reference microcantilevers so that multiple difference signals can be evaluated simultaneously. Thermal drift is cancelled out as one surface of all microcantilevers, typically the lower one, is left uncoated or coated with the same passivation layer.

1.2.4 Deflection Measurement

The bending response of the microcantilever due to adsorption of molecules onto the functional layer is caused by stress formation at the interface be-

tween the functional layer and the forming molecular layer. Because the forces within the functional layer try to keep the distance between molecules constant, the cantilever beam responds by bending because of its extreme flexibility. The quantity describing the flexibility of the microcantilever is its spring constant k. For a rectangular microcantilever of length l, thickness t and width w the spring constant k is calculated as follows:

$$k = \frac{Ewt^3}{4l^3} , \tag{1}$$

where E is Young's modulus ($E_{Si} = 1.3 \times 10^{11}$ N/m^2 for Si(100)).

The microcantilever bends as a response to the formation of surface stress caused by the adsorption of a molecular layer. In its simplest case, the shape of the bent microcantilever can be approximated as part of a circle with radius R. This radius of curvature is given by [12, 13]

$$\frac{1}{R} = \frac{6(1-\nu)}{Et^2} . \tag{2}$$

The resulting surface stress change is described using Stoney's formula [12]:

$$\Delta\sigma = \frac{Et^2}{6R(1-\nu)} , \tag{3}$$

where E is Young's modulus, t the thickness of the cantilever, ν the Poisson's ratio ($\nu_{Si} = 0.24$), and R the bending radius of the cantilever.

The deflection of microcantilever sensors can be measured in various ways. They differ in the sensitivity, the effort for alignment and setup, the robustness and ease of readout, and in the potential for miniaturization.

1.2.4.1 Piezoresistive Readout

Piezoresistive microcantilevers [6, 14] are usually U-shaped and have diffused piezoresistors in both of the legs close to the fixed end. The resistance in the piezoresistors is measured using a Wheatstone bridge circuit with three reference resistors, of which one is adjustable. The current flowing between the two branches of the Wheatstone bridge is first nulled by changing the resistance of the adjustable resistor. If the microcantilever bends, the piezoresistor changes its value and a current will flow between the two branches of the Wheatstone bridge. The current is converted via a differential amplifier into a voltage, which is proportional to the deflection value. For dynamic-mode measurement, the piezoresistive microcantilever is externally actuated via a piezocrystal driven by a frequency generator. The ac actuation voltage is fed as reference voltage into a lock-in amplifier and compared with the response of the Wheatstone bridge circuit allowing to sweep resonance curves and to determine shifts in resonance frequency.

1.2.4.2 Piezoelectric Readout

Piezoelectric microcantilevers [15] are driven via the inverse piezoelectric effect (self-excitation) by applying an electric ac voltage to the piezoelectric material (PZT or ZnO). Sensing of bending is performed by recording the piezoelectric current change taking advantage of the fact that the PZT layer produces a sensitive field response to weak stress through the direct piezoelectric effect. Piezoelectric microcantilevers are multilayer structures consisting of a SiO_2 cantilever and the PZT piezoelectric layer. Two electrode layers, insulated from each other, provide electrical contact. The entire structure is protected using passivation layers. An identical structure is usually integrated into the rigid chip body to provide a reference for the piezoelectric signals from the cantilever.

1.2.4.3 Optical (Beam-Deflection) Readout

The most frequently used approach to read out microcantilever deflections is optical beam deflection [16], because it is a comparatively simple method with an excellent lateral resolution.

The actual cantilever deflection Δx scales with the cantilever dimensions; therefore, deflection responses should be expressed in terms of surface stress $\Delta\sigma$ in N/m to be able to compare cantilever responses acquired with different setups. Various strategies to convert beam deflection signals into stress are described in the literature [17, 18]. Surface stress takes into account the cantilever material properties, such as the Poisson ratio ν, Young's modulus E and the cantilever thickness t. The radius of the curvature R of the cantilever characterizes bending, see Eq. 2. As shown in the drawing in Fig. 2, the actual cantilever displacement Δx is transformed into a displacement Δd on the position sensitive detector (PSD). The position of a light spot on a PSD is determined by measuring the photocurrents from the two facing electrodes. The movement of the light spot on the linear PSD is calculated from the two currents I_1 and I_2 and the size L of the PSD by

$$\Delta d = \frac{I_1 - I_2}{I_1 + I_2} \times \frac{L}{2} \,. \tag{4}$$

As all angles are very small, it can be assumed that the bending angle of the cantilever is equal to half of the angle θ of the deflected laser beam, i.e., $\theta/2$. Therefore, the bending angle of the cantilever can be calculated to be

$$\frac{\theta}{2} = \frac{\Delta d}{2s} \,, \tag{5}$$

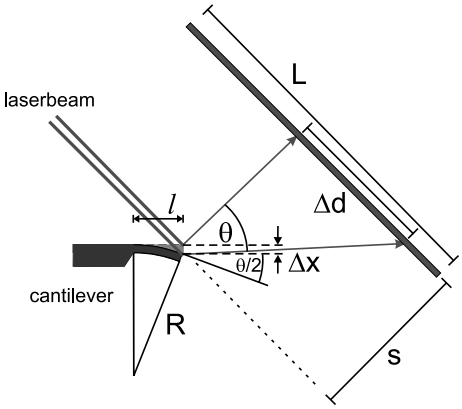

Fig. 2 Beam-deflection concept to determine microcantilever bending with an accuracy of one nanometer

where s is the distance between the PSD and the cantilever. The actual cantilever deflection Δx is calculated from the cantilever length l and the bending angle $\theta/2$ by

$$\Delta x = \frac{\theta/2}{2} \times l \,. \tag{6}$$

The combination of Eqs. 5 and 6 relates the actual cantilever deflection Δx to the PSD signal:

$$\Delta x = \frac{l \times \Delta d}{4s} \,. \tag{7}$$

The relation between the radius of curvature and the deflection angle is

$$\frac{\theta}{2} = \frac{l}{R} \,, \tag{8}$$

and after a substitution becomes

$$R = \frac{2ls}{\Delta d} \quad \text{or} \quad R = \frac{2\Delta x}{l^2} \,. \tag{9}$$

1.3 Realization of an Optical Beam-Deflection Setup

A measurement setup for microcantilever arrays consists of four main parts: 1. the measurement chamber hosting the microcantilever array, 2. an optical or piezoresistive system to detect the cantilever deflection (e.g., laser sources, collimation lenses and a PSD), 3. electronics to amplify, process, and acquire the signals from the PSD, and 4. a gas- or liquid-handling system to reproducibly inject samples into the measurement chamber and purge the chamber.

Figure 3 shows a realization of a setup for experiments performed in (a) liquid (biochemical) and (b) gaseous environment. The microcantilever sensor array is hosted in an analysis chamber of 20 μl in volume, with inlet and outlet ports for gases or liquids, respectively. The bending of the microcantilevers is measured using an array of eight vertical-cavity surface-emitting lasers (VCSELs) arranged at a linear pitch of 250 μm that emit at a wavelength of 760 nm into a narrow cone of 5 to 10°.

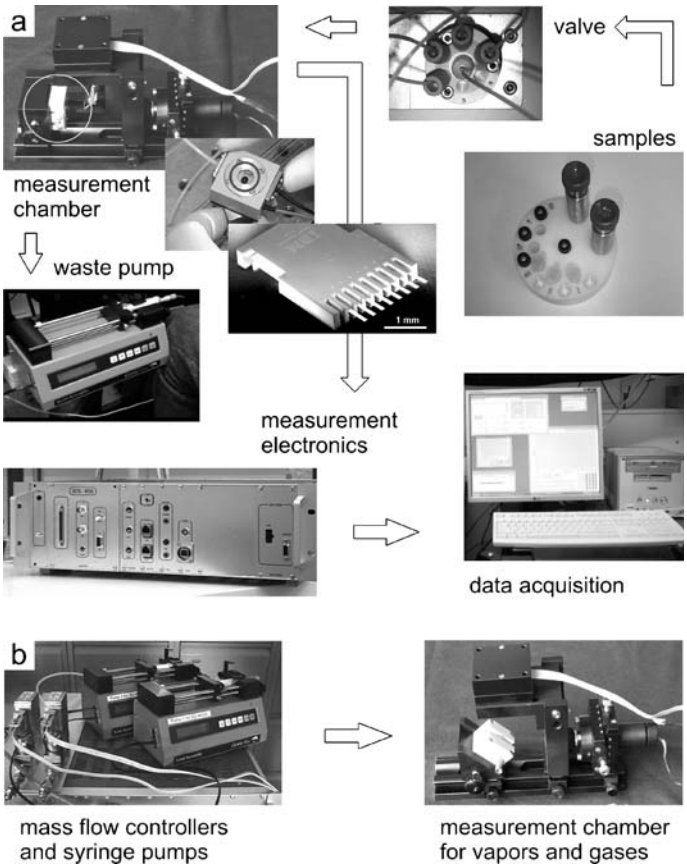

Fig. 3 **a** Realization of a static mode beam-deflection microcantilever-array sensor setup for measurements in liquids. A HPLC 6-way valve is used to select a liquid sample, which is pulled through teflon tubing into the measurement chamber hosting the microcantilever array, until it is collected in the waste pump. The microcantilever bending is measured using optical beam deflection involving VCSELs and a PSD. The location of the laser spot indicating microcantilever bending is processed and digitized using measurement electronics and a data acquisition card in a personal computer. **b** For measurements of vapors and gases the liquid handling system is replaced by a gas handling system consisting of mass flow controllers and syringe pumps for a supply of gaseous samples

The light of each VCSEL is collimated and focused onto the apex of the corresponding microcantilever by a pair of achromatic doublet lenses, 12.5 mm in diameter. This size was selected in order to make sure that all eight laser beams pass through the lenses close to its center in order to minimize scattering, chromatic, and spherical aberration artifacts. The light is then reflected off the gold-coated surface of the cantilever and hits the surface of a PSD. As only a single PSD is used, the eight lasers cannot be switched on simultaneously. Therefore, a time-multiplexing procedure is used to switch the lasers on and off sequentially at typical intervals of 10–100 ms. The resulting deflection signal is digitized and stored together with time information on a personal computer (PC), which also controls the multiplexing of the VCSELs as well as the switching of the valves and mass flow controllers used for setting the composition ratio of the analyte mixture.

The measurement setup for liquids consists of a poly-etheretherketone (PEEK) liquid cell, which contains the cantilever array and is sealed by a viton O-ring and a glass plate. The VCSELs and the PSD are mounted on a metal frame around the liquid cell. After preprocessing the position of the deflected light beam using a current-to-voltage converter and amplifier stage, the signal is digitized in an analog-to-digital converter and stored on a PC. The liquid cell is equipped with inlet and outlet ports for liquids. They are connected via 0.18 mm of i.d. teflon tubing to individual thermally-equilibrated glass containers, in which the biochemical liquids are stored. A six-position valve allows the inlet to the liquid chamber to be connected to each of the liquid-sample containers separately. The liquids are pulled through the liquid chamber by means of a syringe pump connected to the outlet of the chamber. A peltier element located beneath the microcantilever array in the PEEK chamber allows regulating the temperature within the chamber. The entire experimental setup is housed in a temperature-controlled box regulated with an accuracy of 0.01 K to the target temperature.

2 Operating Modes

A microcantilever sensor is a versatile tool for the investigation of various sample properties and allows to follow reactions occurring on its surface. Various operating modes have been presented.

2.1 Static Mode

Gradual bending of a microcantilever with molecular coverage is referred to as operation in the “static mode”. Various environments are possible, such as vacuum, ambient environment, and liquids. In a gaseous environment,

molecules adsorb on the functionalized sensing surface and form a molecular layer, provided there is affinity for the molecules to adhere to the surface. Polymer sensing layers show a partial sensitivity, because molecules from the environment diffuse into the polymer layer at different rates, mainly depending on the size and solubility of the molecules in the polymer layer. By selecting polymers among a wide range of hydrophilic/hydrophobic ligands, the chemical affinity of the surface can be influenced, because different polymers vary in diffusion suitability for polar/unpolar molecules. Thus, for detection in the gas phase, the polymers can be chosen according to the detection problem, i.e. what the applications demand. Typical chemicals to be detected are volatile organic compounds (VOCs).

Static-mode operation in liquids, however, usually requires rather specific sensing layers, based on molecular recognition, such as DNA hybridization or antigen-antibody recognition.

2.2 Dynamic Mode

If the molecules adsorb as a monolayer, the coverage and therewith the mass adsorbed can be determined from the static deflection signal. More generally, information on the amount of molecules adsorbed can be obtained by oscillating the microcantilever at its eigenfrequency. However, the surface coverage is basically not known. Furthermore, molecules on the surface might be exchanged with molecules from the environment in a dynamic equilibrium.

In contrast, mass changes can be determined accurately by tracking the eigenfrequency of the microcantilever during mass adsorption or desorption. The eigenfrequency equals the resonance frequency of an oscillating microcantilever if its elastic properties remain unchanged during the molecule adsorption/desorption process and damping effects are negligible. This operation mode is called the dynamic mode. The microcantilever is used as a microbalance, as with mass addition on the cantilever surface, the cantilever's eigenfrequency will shift to a lower value. The mass change on a rectangular cantilever is calculated [9] according to

$$\Delta m = (k/4\pi^2) \times (1/f_1^2 - 1/f_0^2)\,, \tag{10}$$

where f_0 is the eigenfrequency before the mass change occurs, and f_1 the eigenfrequency after the mass change. For the calculation of the spring constant k of the cantilever see Eq. 1.

Mass-change determination can be combined with varying environment temperature conditions to obtain a method introduced in the literature as "micromechanical thermogravimetry" [14]. The sample to be investigated is mounted onto the cantilever. Its mass should not exceed several hundred nanograms. In case of adsorption, desorption, or decomposition processes,

mass changes in the picogram range can be observed in real time by tracking the resonance-frequency shift.

Dynamic mode operation in a liquid environment poses problems, such as high damping of the cantilever oscillation due to the high viscosity of the surrounding media. This results in a low quality factor Q of the oscillation, and the resonance frequency shift is difficult to track with high resolution. The quality factor is defined as

$$Q = 2\Delta f / f_0 \,, \tag{11}$$

whereas in air a frequency resolution of below 1 Hz is easily achieved, resolution values of about 20 Hz are already to be considered very good for measurements in a liquid environment. In the case of damping or changes of the elastic properties of the cantilever during the experiment, e.g., a stiffening or softening of the spring constant by adsorption of a molecule layer, the measured resonance frequency will not be exactly the same as the eigenfrequency, and the mass derived from the frequency shift will be inaccurate. Unlike in ultrahigh vacuum conditions [19, 20], where resonance frequency is equal to eigenfrequency, these terms should be carefully distinguished for operation in a large damping environment, as described, for example, in [21].

2.3 Heat Mode

For a microcantilever that is coated with metal layers, thermal expansion differences in cantilever and coating layer will have to be taken into account, as they will further influence cantilever bending as a function of temperature. This mode of operation is referred to as "heat mode" and causes cantilever bending because of differing thermal expansion coefficients in sensor layer and cantilever materials [8]:

$$\Delta z = 1.25 \times (\alpha_1 - \alpha_2) \times (t_1 + t_2)/t_2^2 \kappa \times l^3 P/(\alpha_1 t_1 + \alpha_2 t_2) w \,. \tag{12}$$

Here α_1, α_2 are the thermal expansion coefficients of the microcantilever and coating materials, t_1, t_2 the material thicknesses, P is the total power generated on the cantilever, and κ a geometry parameter of the cantilever device.

Heat changes are either caused by external influences, such as a change in temperature, occur directly on the surface by exothermal, e.g., catalytic, reactions, or are due to material properties of a sample attached to the apex of the cantilever (micromechanical calorimetry). The sensitivity of the cantilever heat mode is orders of magnitude higher than that of traditional calorimetric methods performed on milligram samples, as it only requires nanogram amounts of sample and achieves nanojoules [9] to picojoules [22, 23] sensitivity.

These three measurement modes have established cantilevers as versatile tools to perform experiments in nanoscale science with very small amounts of material.

2.4 Photothermal Spectroscopy

When a material adsorbs photons, a fraction of energy is converted into heat. This photothermal heating can be measured as a function of the light wavelength to provide optical absorption data of the material. The interaction of light with a bimetallic cantilever creates heat on the cantilever surface, resulting in a bending of the cantilever [24]. Such bimetallic-cantilever devices are capable of detecting heat flows due to an optical heating power of 100 pW, being two orders of magnitude better than in conventional photothermal spectroscopy.

2.5 Electrochemistry

A cantilever coated with a metallic layer (a measurement electrode) on one side is placed in an electrolytic medium, e.g., a salt solution, together with a metallic reference electrode, usually made of a noble metal. Variations of the voltage between measurement and reference electrode induce electrochemical processes on the measurement electrode (cantilever), e.g., the adsorption or desorption of ions from the electrolyte solution onto the measurement electrode. These processes lead to a bending of the cantilever according to the Shuttleworth equation relating stress, surface energy, and its derivative with respect to strain [25].

3 Functionalization

It is essential that the surfaces of the cantilever are coated in a proper way to provide suitable receptor surfaces for the molecules to be detected. Such coatings should be specific, homogeneous, stable, reproducible, and either reusable or designed for single use only. For static mode measurements, one side of the cantilever should be passivated for blocking unwanted adsorption. Often, the cantilever's upper side, the sensor side, is coated with a 20 nm thick layer of gold to provide a platform for the binding of receptor molecules, for example via thiol chemistry, whereas the lower side is passivated using silane chemistry for coupling an inert surface such as poly-ethylene glycol silane. Silanization is performed first on the silicon microcantilever. Then, a gold layer is deposited on the top side of the cantilever, leaving the lower side un-

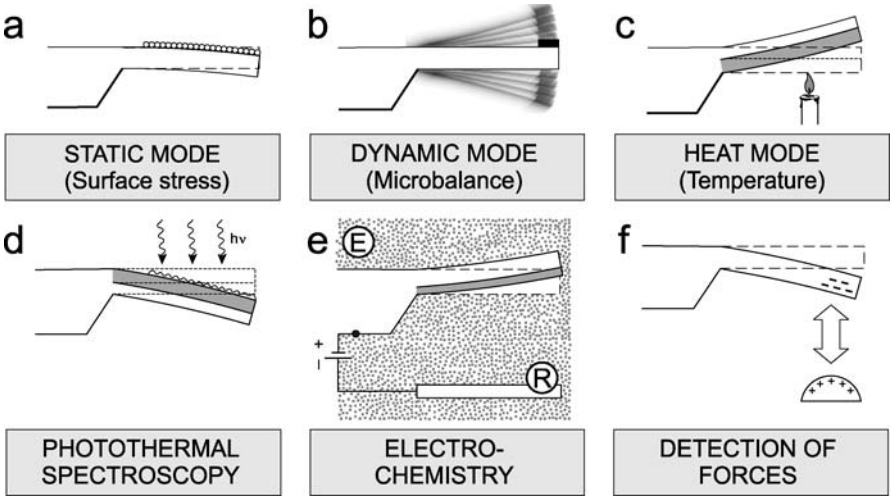

Fig. 4 Major operating modes of microcantilever sensors: **a** static mode exploiting surface stress changes, **b** dynamic mode to extract mass changes, **c** heat mode for determining phase transitions and heat capacity effects of a sample attached to the cantilever, **d** photothermal spectroscopy taking advantage of light-induced interactions with the cantilever coating, **e** electrochemistry, **f** detection of forces between the microcantilever and an external sample

changed. It is very important that the method of choice is fast, reproducible, reliable, and allows one or both cantilever surfaces to be coated separately. Various ways are reported to coat a cantilever with molecular layers. Here, two different strategies are highlighted.

3.1
Coating in Microcapillary Arrays

A convenient method to coat microcantilevers with probe molecules is the insertion of the cantilever array into an array of dimension-matched disposable glass capillaries. The outer diameter of the glass capillaries is 240 μm so that they can be placed neatly next to each other to accommodate the pitch of the cantilevers in the array (250 μm). Their inner diameter is 150 μm, allowing sufficient room to insert the cantilevers (width: 100 μm) safely (Fig. 5). This method has been successfully applied for the deposition of a variety of materials onto cantilevers, such as polymer solutions [26], self-assembled monolayers [27], thiol-functionalized single-stranded DNA oligonucleotides [28–30], and proteins [31, 32]. Incubation of the microcantilever array in the microcapillaries takes from a few seconds (the self-assembly of alkanethiol monolayers) to several tens of minutes (coating with protein solutions). The microcapillary functionalization unit may be placed in an environment of sat-

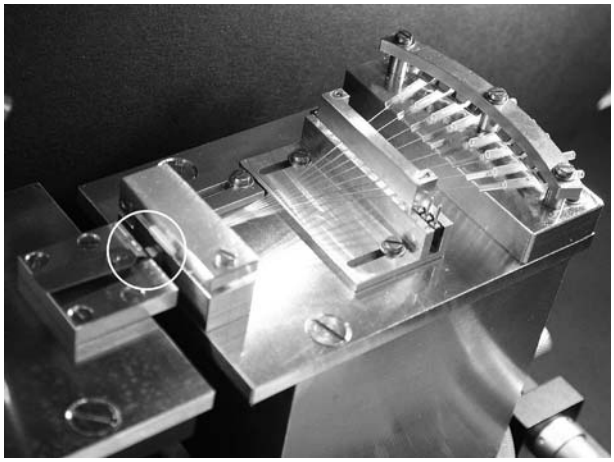

Fig. 5 Functionalization stage for coating microcantilevers with self-assembled monolayers, for example. Microcapillaries filled with the solutions containing the probe molecules transport the liquid via capillarity to the cantilevers, whereby each microcantilever is inserted into one microcapillary. Therefore, no cross-contanination of liquids will occur. The location of the microcantilever array is indicated by a circle

urated vapor of the solvent used for the probe molecules to avoid drying out of the solutions.

3.2 Coating Using an Inkjet Spotter

Coating in microcapillary arrays requires the manual alignment of the microcantilever array and the functionalization tool, and is therefore not suitable for coating large numbers of cantilever arrays. Moreover, upper and lower surface of microcantilevers are exposed to the solution containing the probe molecules. For ligands that bind covalently, e.g., by gold-thiol coupling, only the upper surface will be coated, provided the gold layer has only be applied on the upper surface of the microcantilever. For coating with polymer layers, microcapillary arrays are not suitable, because both surfaces of the microcantilever would be coated with polymer layers, being inappropriate for static mode measurements, where an asymmetry between the upper and lower surface is required.

A method appropriate for coating many cantilever sensor arrays in a rapid and reliable way is inkjet spotting [33, 34]; see Fig. 6. An x–y–z positioning system allows a fine nozzle (capillary diameter: 70 μm) to be positioned with an accuracy of approx. 10 μm over a cantilever. Individual droplets (diameter: 60–80 μm, volume 0.1–0.3 nl) can be dispensed individually by means of a piezo-driven ejection system in the inkjet nozzle. When the droplets

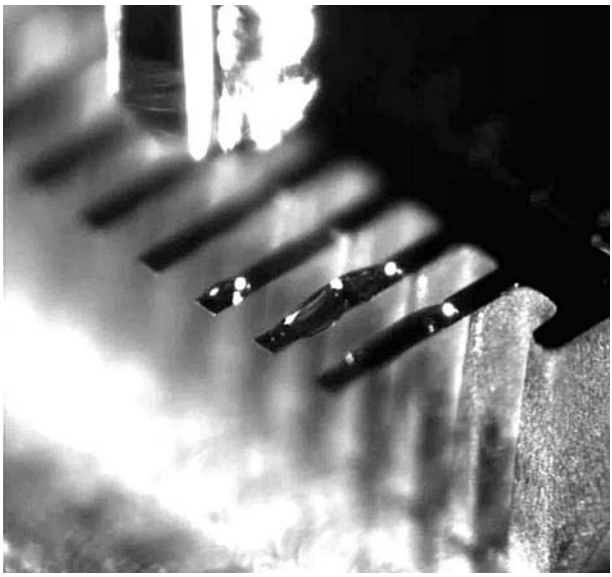

Fig. 6 Single-sided microcantilever coating using an inkjet spotter. The amount of liquid containing the probe molecules can be dosed accurately by choosing the number of drops being ejected from the nozzle

are spotted with a pitch smaller than 0.1 mm, they merge and form continuous films. By adjusting the number of droplets deposited on cantilevers, the resulting film thickness can be controlled precisely. The inkjet-spotting technique allows a cantilever to be coated within seconds and yields very homogeneous, reproducibly deposited layers of well-controlled thickness. The suc-

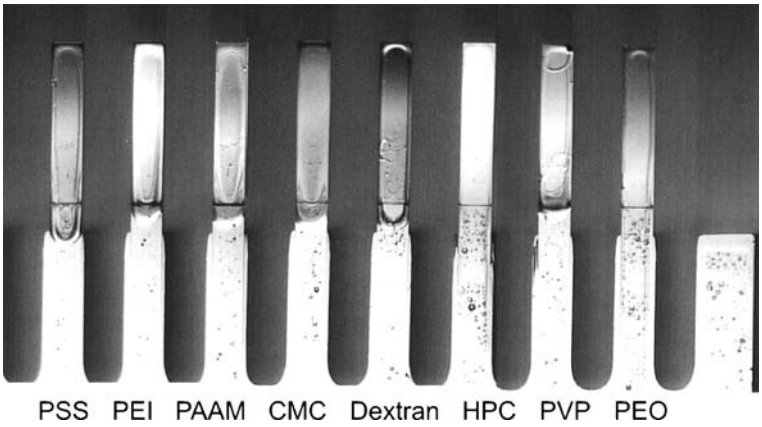

Fig. 7 Optical microscopy image of a polymer-coated microcantilever array for application as an artificial nose for solvents. The pitch between microcantilevers is 250 micron

cessful coating of self-assembled alkanethiol monolayers, polymer solutions, self-assembled DNA single-stranded oligonucleotides [34], and protein layers has been demonstrated. Figure 7 shows a polymer coated microcantilever array for the chemical vapor detection experiments described in the following section. In conclusion, inkjet spotting has turned out to be a very efficient and versatile method for functionalization that can even be used to coat arbitrarily-shaped sensors reproducibly and reliably [35, 36].

4
Applications

The applications of microcantilever sensors are manifold: gas sensing, the quality control of chemicals, food, and air as well as process monitoring and control, just to give a few examples. As an artificial nose, cantilever array sensors can characterize odors and vapors and may be used to assist fragrance design. Due to its extremely high sensitivity, the technique has a large potential to be applied for drugs and explosives detection, as well as for forensic investigations. In a liquid environment, its major applications are in biochemical analysis and medical diagnosis.

4.1
Chemical Vapor Detection

Sensors for the reliable detection of solvent vapors are important in chemical process technology, e.g., for safe handling during storage and the transport of large amounts of solvents in containers. A fast test is needed to identify solvents in transport containers. Such a test might be realized using polymer-coated microcantilever sensors. In a laboratory setup, 0.1 ml of various solvents was placed in vials, and the vapor from the headspace above the liquid was sampled using microcantilever sensors, operated in static deflection mode as a kind of artificial nose. The detection of vapors takes place via the diffusion of the vapor molecules into the polymer, resulting in a swelling of the polymer and a bending of the cantilever. Each cantilever is coated with a different polymer or polymer blend (see Fig. 7). The bending is specific for the interaction between solvent vapor and polymer time- and magnitude-wise.

Cantilever deflection traces upon subsequent injection of solvent vapor for 30 s and purging with dry nitrogen for 150 s are shown in Fig. 8 for (a) water, (b) ethanol, and (c) methanol.

The cantilever deflections at 10, 20, 30, and 40 seconds after the completion of the solvent vapor injection are extracted. They describe the time-development of the curves in a reduced data set, i.e., $8 \times 4 = 32$ cantilever deflection amplitudes ("fingerprint") that account for a measurement data set. This data set is then evaluated using principal component analysis (PCA)

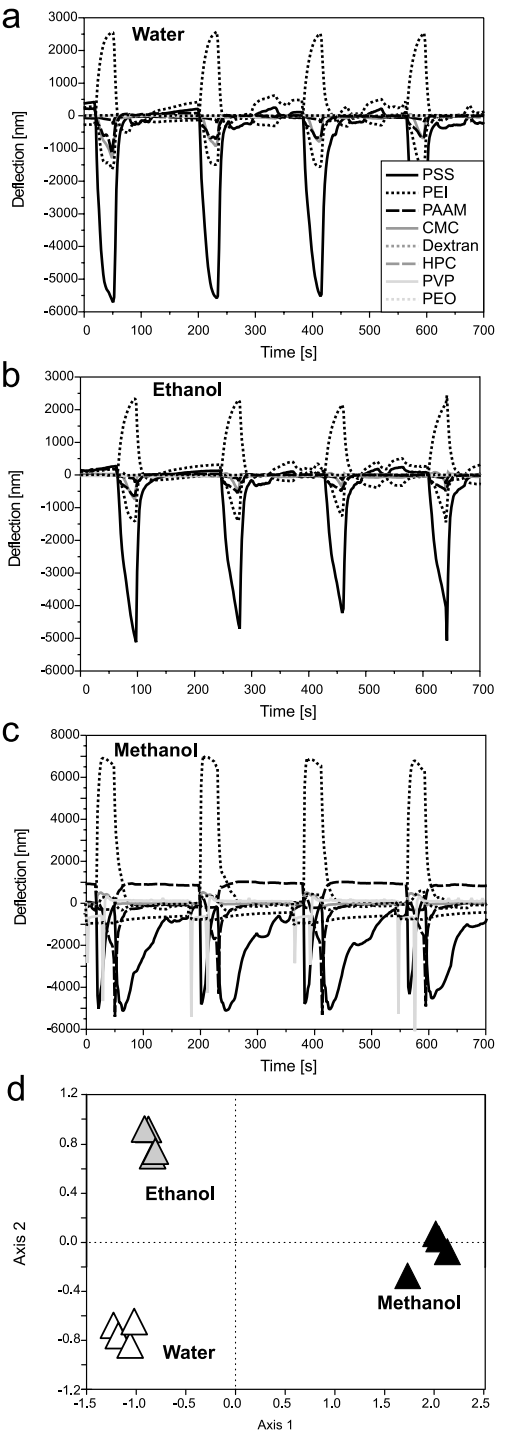
a
Water
Deflection [nm]
Time [s]
PSS
PEI
PAAM
CMC
Dextran
HPC
PVP
PEO
b
Ethanol
Deflection [nm]
Time [s]
c
Methanol
Deflection [nm]
Time [s]
d
Ethanol
Methanol
Water
Axis 2
Axis 1

◀ **Fig. 8** Application of microcantilever array sensors as an artificial electronic nose. Measurement traces of microcantilevers coated with polymers during the detection of **a** water, **b** ethanol, **c** methanol. For every solvent, four consecutive injections of vapor saturated with solvent are shown. Upon injection of solvent vapor, the microcantilevers deflect in a specific way due to the swelling of the polymer layer on exposure to the solvent vapor. Subsequent purging of the measurement chamber with dry nitrogen gas (flow rate: 100 ml/min) promotes diffusion of the solvent molecules out of the polymer layer, resulting in a bending back of the microcantilevers to the baseline. **d** Principal component analysis (PCA) of the response patterns of all eight microcantilevers upon exposure to the three different solvent vapors. Clear separation of the clusters proves the excellent distinction capability of the artificial nose setup. Each symbol in the PCA plot corresponds to one of the injections in **a**–**c**

techniques, extracting the most dominant deviations in the responses for the various sample vapors. The axes refer to projections of the multidimensional datasets into two dimensions (principal components). The labels in the PCA plot (Fig. 8d) indicate the individual measurements. The PCA plot shows well-separated clusters of measurements indicating the clear identification of vapor samples. Even vapor mixtures can be analyzed using PCA [37].

4.2 Explosives Detection

A large effort is also put into the development of inexpensive, highly selective, and very sensitive small sensors that can be mass-produced and microfabricated. Current miniaturized versions, including ion mobility spectrometers [38] or nuclear quadrupole resonance [39] are bulky. Microcantilever sensors offer sensitivities more than two orders of magnitude better than quartz crystal microbalances [40], flexural plate wave oscillators [41], and surface acoustic wave devices [42]. Several approaches to detect dangerous chemicals are already described in the literature: photomechanical chemical microsensors based on adsorption-induced and photo-induced stress changes due to the presence of diisopropyl methyl phosphonate (DIMP), which is a model compound for phosphorous-containing chemical warfare agents, and trinitrotoluene (TNT), an explosive [43]. Further explosives frequently used include pentaerythritol tetranitrate (PETN) and hexahydro-1,3,5-triazine (RDX), often also with plastic fillers [44]. These compounds are very stable, if no detonator is present. Their explosive power, however, is very large, and moreover, the vapor pressures of PETN and RDX are very low, in the range of ppb and ppt. By functionalizing microcantilevers with self-assembled monolayers of 4-mercaptobeonzoic acid (4-MBA) PETN was detected at a level of 1400 ppt and RDX at a level of 290 ppt [44]. TNT was found to readily stick to Si surfaces, suggesting the use of microcantilevers for TNT detection, taking advantage of the respective adsorption/desorption kinetics [45, 46]. The detection of TNT via deflagration on a microcantilever is de-

Table 1 Polymer coatings

Cantilever	Polymer	Full name of compound
1	PSS	Poly(sodium 4-styrenesulfonate)
2	PEI	Polyethylenimine
3	PAAM	Poly(allylamine hydrochloride)
4	CMC	Carboxymethylcellulose sodium salt
5	Dextran	Dextran from Leuconostoc spp.
6	HPC	Hydroxypropyl cellulose
7	PVP	Polyvinylpyrrolidone
8	PEO	Poly(2-ethyl-2-oxazoline)

scribed by Pinnaduwage et al. [47]. They used piezoresistive microcantilevers where the cantilever deflection was measured optically via beam deflection. TNT vapor from a generator placed 5 mm away from the microcantilever was observed to adsorb on its surface resulting in a decrease of resonance frequency. Application of an electrical pulse (10 V, 10 ms) to the piezoresistive cantilever resulted in deflagration of the TNT vapor and a bump in the cantilever bending signal. This bump was found to be related to the heat produced during deflagration. The amount of heat released is proportional to the area of the bump in the time vs. bending signal diagram of the process. The deflagration was found to be complete, as the same resonance frequency as before the experiment was observed. The amount of TNT mass involved was determined as 50 pg. The technique was later extended to the detection of PETN and RDX, where a much slower reaction kinetics was observed [48, 49]. Traces of 2,4-dinitrotoluene (DNT) in TNT can also be used for detection of TNT, because it is the major impurity in production grade TNT. Furthermore DNT is a decomposition product of TNT. The saturation concentration of DNT in air at 20 °C is 25 times higher than that of TNT. DNT was reported to be detected at the 300 ppt level using polysiloxane polymer layers [50]. The microfabrication of electrostatically actuated resonant microcantilever beams in CMOS technology for detection of the nerve agent stimulant dimethylmethylphosphonate (DMMP) using polycarbosilane-coated beams [51] is an important step towards an integrated platform based on silicon microcantilevers, which, besides compactness, might also include telemetry [52].

5
Recent Literature and Outlook

In recent years the field of cantilever sensors has been very active. Some recent developments are reviewed in [53–58]. Major topics published include the following studies: the fabrication of silicon piezoresistive [59, 60] or

polymer [61] cantilevers, detection of vapors and volatile compounds, e.g., mercury vapor [62], HF vapor [63, 64], chemical vapors [65], as well as the development of gas sensors based on the piezoresistive concept [66]. Pd-based sensors for hydrogen [67], deuterium and tritium [68] are reported, as well as sensors taking advantage of the sensing properties of hydrogels [69] or zeolites [70]. A humidity sensor is suggested in [71]. A field of growing interest is the detection of explosives [47], pathogens [72], nerve agents [73], viruses [74], bacteria, e.g., E. coli, [75], and pesticides such as dichlorodiphenyltrichloroethane (DDT) [76]. The issues of detection of environmental pollutants are discussed in [77]. A chemical vapor sensor based on the bimetal technique is described in [78]. The measurement of electrochemical redox reactions with cantilevers is reported [79]. In biochemical applications, detection of DNA [80, 81], proteins [82], prostate-specific antigen (PSA) [83], peptides using antibodies [84] and living cells [85] is possible. Medical applications involve diagnostics [86], drug discovery [87], and the detection of glucose [88]. To increase the complexity of microcantilever applications, two-dimensional microcantilever arrays have been proposed for multiplexed biomolecular analysis [89, 90].

For measurements in gaseous environment, a sensor application in dynamic mode of piezoelectric cantilevers for an ultrasensitive nanobalance is reported [91]. Micromolded plastic microcantilevers are proposed for chemical sensing [92], as well as micromachined silicon microcantilevers for gas sensing based on capacitive read-out [93]. In chemical sensing, ligand-functionalized microcantilevers for characterization of metal ion sensing are presented [94], and an array of flexible microcantilever beams is used to observe the action of rotaxane based artificial molecular muscles [95]. The importance of homeland security is discussed in [51], where electrostatically actuated resonant microcantilever beams in CMOS technology are utilized for the detection of chemical weapons. An integrated sensor platform for homeland defense based on silicon microcantilevers is described in [52]. In the field of electrochemistry, microcantilevers have been used to measure redox-induced surface stress [96], and a differential microcantilever-based system for measuring surface stress changes induced by electrochemical reactions has been presented [97].

Many publications concern biochemical applications, such as a label-free immunosensor array using single-chain antibody fragments [32] and the label-free analysis of transcription factors using microcantilever arrays [98]. Microcantilevers modified by horseradish peroxidase intercalated nano-assembly have been applied for hydrogen peroxide detection [99], and the detection of cystamine dihydrochloride and glutaraldehyde [100, 101]. Furthermore, a back-propagation artificial neural network recognition study of analyte species and concentration has been presented [102].

Cantilever sensors for nanomechanical detection have been used for the observation of specific protein conformation changes [103]. In the field of

DNA hybridization detection, the chemomechanics of surface stresses induced by DNA hybridization has been studied [104] and the grafting density and binding efficiency of DNA and proteins on gold surfaces has been characterized and improved [105]. An electrostatic microcantilever array biosensor has been applied for DNA detection [106], and microcantilever sensors for DNA hybridization reactions or antibody-antigen interactions without using external labels have been tested in dynamic mode [107].

An immunoassay of prostate-specific antigen (PSA) exploiting the resonant frequency shift of piezoelectric nanomechanical microcantilevers is reported [108], as well as phospholipid vesicle adsorption measured in situ using resonating cantilevers in a liquid cell [109]. Microcantilevers have been utilized to detect bacillus anthracis [110], and glucose oxidase multilayer modified microcantilevers can measure glucose [111].

Effort has been put into the refinement of the cantilever sensor method: a dimension dependence study of the thermomechanical noise of microcantilevers is available to determine the minimal detectable force and surface stress [112]. Furthermore, the geometrical and flow configurations for enhanced microcantilever detection within a fluidic cell have been investigated [113]. A microcapillary pipette-assisted method to prepare polyethylene glycol-coated microcantilever sensors has been suggested [114] and the role of material microstructure in plate stiffness with relevance to microcantilever sensors has been studied [115]. Double-sided surface stress cantilever sensors for more sensitive cantilever surface stress measurement have been proposed [116].

Enhanced microcantilever sensor techniques involve a biosensor based on magnetostrictive microcantilevers [117], the piezoelectric self-sensing of adsorption-induced microcantilever bending [118], the optical sequential readout of microcantilever arrays for biological detection achieved by scanning the laser beam [119], and cysteine monolayer modified microcantilevers to monitor flow pulses in a liquid [120]. The photothermal effect has been used to study dynamic elastic bending in microcantilevers [121]. For dynamic mode, temperature and pressure dependence of resonance in multi-layer microcantilevers have been investigated [122] and the inaccuracy in the detection of molecules has been discussed [123].

The influence of surface stress on the resonance behavior of microcantilevers in higher resonant modes has been studied [124] and an alternative solution has been proposed to improve the sensitivity of resonant microcantilever chemical sensors by measuring in high-order modes and reducing geometrical dimensions [125]. A modal analysis of microcantilever sensors with environmental damping is reported [126]. Furthermore, theoretical work is available on the simulation of adsorption-induced stress of a microcantilever sensor [127], the influence of nanobubbles on the bending of microcantilevers [128], the modeling and simulation of thermal effects in flexural microcantilever resonator dynamics [129], and surface stress effects related to

the resonance properties of cantilever sensors [130]. Further information about the origin of the signal in microcantilever sensors, especially diffusion properties, is found in [131]. Finally, a review on nanotechnologies for biomolecular detection and medical diagnostics appeared [132].

Cantilever array sensors might be one of the solutions to the demand for miniaturized, ultrasensitive and fast-responsive sensors for application in gas detection, and surveillance, as well as in biochemistry and medicine. For their reliable use, some technical issues have still to be resolved, e.g., the simplification of the alignment procedure, which is related to the optical beam deflection readout. Here, the integration possibilities with piezoresistive microcantilevers are much higher than for those based on optical beam-deflection. Silicon nitride coating [133] is a promising strategy to obtain the durable protection of piezoresistive microcantilevers, even in biochemical solutions.

Furthermore, the periphery for measurements with microcantilever array sensors is required to be miniaturized as well, whereby microfluidic concepts have to be integrated with the microcantilever array. Further downscaling is theoretically favorable as the sensitivity of the devices improves, but it also poses technical challenges to determine deflection signals from such tiny structures. The use of a few hundred nanometer long and a few ten nanometer thick nanocantilevers has been reported to yield a dramatical increase in performance [134, 135], but their practical use becomes very complicated, e.g., as far as the functionalization, the sample handling, and the readout are concerned. The field is open to welcome completely new ideas for efficient working procedures for nanocantilever sensors.

Acknowledgements We thank R. McKendry (University College London, London, U.K.), M. Hegner, W. Grange, Th. Braun, J. Zhang, A. Bietsch, V. Barwich, M. Ghatkesar, F. Huber, N. Backmann, J.-P. Ramseyer, A. Tonin, H.R. Hidber, E. Meyer and H.-J. Güntherodt (University of Basel, Basel, Switzerland) for valuable contributions and discussions, as well as U. Drechsler, M. Despont, H. Schmid, E. Delamarche, H. Wolf, R. Stutz, R. Allenspach, and P.F. Seidler (IBM Research, Zurich Research Laboratory, Rüschlikon, Switzerland). We also thank the European Union FP 6 Network of Excellence FRONTIERS for support. This project is funded partially by the National Center of Competence in Research in Nanoscience (Basel, Switzerland), the Swiss National Science Foundation and the Commission for Technology and Innovation (Bern, Switzerland).

References

1. Wilfinger RJ, Bardell PH, Chhabra DS (1968) IBM J Res Dev 12:113
2. Heng TMS (1971) IEEE Trans Microwave Theory Techn 19:652
3. Petersen KE (1979) IBM J Res Develop 23:376
4. Kolesar ES (1983) US Patent 4 549 427
5. Binnig G, Quate CF, Gerber C (1986) Phys Rev Lett 56:930
6. Itoh T, Suga T (1994) Appl Phys Lett 64:37
7. Cleveland JP, Manne S, Bocek D, Hansma PK (1993) Rev Sci Instrum 64:403
8. Gimzewski JK, Gerber C, Meyer E, Schlittler RR (1994) Chem Phys Lett 217:589

9. Thundat T, Warmack RJ, Chen GY, Allison DP (1994) Appl Phys Lett 64:2894
10. Thundat T, Chen GY, Warmack RJ, Allison DP, Wachter EA (1995) Anal Chem 67:519
11. Lang HP, Berger R, Andreoli C, Brugger J, Despont M, Vettiger P, Gerber C, Gimzewski J, Ramseyer JP, Meyer E, Güntherodt HJ (1998) Appl Phys Lett 72:383
12. Stoney GG (1909) Proc R Soc London, Ser A 82:172
13. von Preissig FJ (1989) J Appl Phys 66:4262
14. Berger R, Lang HP, Gerber C, Gimzewski JK, Fabian JH, Scandella L, Meyer E, Güntherodt HJ (1998) Chem Phys Lett 294:363
15. Lee C, Itoh T, Ohashi T, Maeda R, Suga T (1997) J Vac Sci Technol B 15:1559
16. Meyer G, Amer NM (1988) Appl Phys Lett 53:2400
17. Jeon S, Jung N, Thundat T (2007) Sens Actuators B 122:365
18. Godin M, Williams PJ, Tabard-Cossa V, Laroche O, Beaulieu LY, Lennox RB, Grutter P (2004) Langmuir 20:7090
19. Ekinci KL, Roukes ML (2005) Rev Sci Instr 76:061101
20. Ilic B, Craighead HG, Krylov S, Senaratne W, Ober C, Neuzil P (2004) J Appl Phys 95:3694
21. Braun T, Barwich V, Ghatkesar MK, Bredekamp AH, Gerber C, Hegner M, Lang HP (2005) Phys Rev E 72:031907
22. Bachels T, Schäfer R (1999) Chem Phys Lett 300:177
23. Bachels T, Tiefenbacher F, Schäfer R (1999) J Chem Phys 110:10008
24. Barnes JR, Stephenson RJ, Welland ME, Gerber C, Gimzewski JK (1994) Nature 372:79
25. Tabard-Cossa V, Godin M, Burgess IJ, Monga T, Lennox RB, Grutter P (2007) Anal Chem 79:8136
26. Baller MK, Lang HP, Fritz J, Gerber C, Gimzewski JK, Drechsler U, Rothuizen H, Despont M, Vettiger P, Battiston FM, Ramseyer JP, Fornaro P, Meyer E, Güntherodt HJ (2000) Ultramicroscopy 82:1
27. Fritz J, Baller MK, Lang HP, Strunz T, Meyer E, Güntherodt HJ, Delamarche E, Gerber C, Gimzewski JK (2000) Langmuir 16:9694
28. Fritz J, Baller MK, Lang HP, Rothuizen H, Vettiger P, Meyer E, Güntherodt HJ, Gerber C, Gimzewski JK (2000) Science 288:316
29. McKendry R, Zhang J, Arntz Y, Strunz T, Hegner M, Lang HP, Baller MK, Certa U, Meyer E, Güntherodt HJ, Gerber C (2002) Proc Natl Acad Sci USA 99:9783
30. Zhang J, Lang HP, Huber F, Bietsch A, Grange W, Certa U, McKendry R, Güntherodt HJ, Hegner M, Gerber C (2006) Nat Nanotechn 1:214
31. Arntz Y, Seelig JD, Lang HP, Zhang J, Hunziker P, Ramseyer JP, Meyer E, Hegner M, Gerber C (2003) Nanotechnology 14:86
32. Backmann N, Zahnd C, Huber F, Bietsch A, Plückthun A, Lang HP, Güntherodt HJ, Hegner M, Gerber C (2005) Proc Natl Acad Sci USA 102:14587
33. Bietsch A, Hegner M, Lang HP, Gerber C (2004) Langmuir 20:5119
34. Bietsch A, Zhang J, Hegner M, Lang HP, Gerber C (2004) Nanotechnology 15:873
35. Lange D, Hagleitner C, Hierlemann A, Brand O, Baltes H (2002) Anal Chem 74:3084
36. Savran CA, Burg TP, Fritz J, Manalis SR (2003) Appl Phys Lett 83:1659
37. Taurino AM, Distante C, Siciliano P, Vasanelli L (2003) Sens Actuators B 93:117
38. Ewing RG, Miller CJ (2001) Field Anal Chem Technol 5:215
39. Garroway AN, Buess ML, Miller JB, Suits BH, Hibbs AD, Barrall GA, Matthews R, Burnett LJ (2001) IEEE Trans Geosci Remote Sens 39:1108
40. O'Sullivan CK, Guilbault GG (1999) Biosens Bioelectron 14:663
41. Cunningham B, Weinberg M, Pepper J, Clapp C, Bousquet R, Hugh B, Kant R, Daly C, Hauser E (2001) Sens Actuators B 73:112

42. Grate JW (2000) Chem Rev 100:2627 (Washington, DC)
43. Datskos PG, Sepaniak MJ, Tipple CA, Lavrik N (2001) Sens Actuators B 76:393
44. Pinnaduwage LA, Boiadjiev V, Hawk JE, Thundat T (2003) Appl Phys Lett 83:1471
45. Muralidharan G, Wig A, Pinnaduwage LA, Hedden D, Thundat T, Lareau RT (2003) Ultramicroscopy 97:433
46. Pinnaduwage LA, Yi D, Tian F, Thundat T, Lareau RT (2004) Langmuir 20:2690
47. Pinnaduwage LA, Wig A, Hedden DL, Gehl A, Yi D, Thundat T, Lareau RT (2004) J Appl Phys 95:5871
48. Pinnaduwage LA, Thundat T, Gehl A, Wilson SD, Hedden DL, Lareau RT (2004) Ultramicroscopy 100:211
49. Pinnaduwage LA, Gehl A, Hedden DL, Muralidharan G, Thundat T, Lareau RT, Sulchek T, Manning L, Rogers B, Jones M, Adams JD (2003) Nature 425:474
50. Pinnaduwage LA, Thundat T, Hawk JE, Hedden DL, Britt R, Houser EJ, Stepnowski S, McGill RA, Bubb D (2004) Sens Actuators B 99:223
51. Voiculescu I, Zaghloul ME, McGill RA, Houser EJ, Fedder GK (2005) IEEE Sensors J 5:641
52. Pinnaduwage LA, Ji HF, Thundat T (2005) IEEE Sensors J 5:774
53. Majumdar A (2002) Disease Markers 18:167
54. Lavrik NV, Sepaniak MJ, Datskos PG (2004) Rev Sci Instrum 75:2229
55. Ziegler C (2004) Anal Bioanal Chem 379:946
56. Hansen KM, Thundat T (2005) Methods 37:57
57. Carrascosa LG, Moreno M, Alvarez M, Lechuga LM (2005) TRAC-Trends Anal Chem 25:196
58. Yan XD, Ji HF, Thundat T (2006) Curr Anal Chem 2:297
59. Tang YJ, Fang J, Yan XD, Ji HF (2004) Sens Actuators B 97:109
60. Forsen E, Nilsson SG, Carlberg P, Abadal G, Perez-Murano F, Esteve J, Montserrat J, Figueras E, Campabadal F, Verd J, Montelius L, Barniol N, Boisen A (2004) Nanotechnology 15:S628
61. McFarland AW, Poggi MA, Bottomley LA, Colton JS (2004) Rev Sci Instrum 75:2756
62. Rogers B, Manning L, Jones M, Sulchek T, Murray K, Beneschott B, Adams JD, Hu Z, Thundat T, Cavazos H, Minne SC (2003) Rev Sci Instrum 74:4899
63. Mertens J, Finot E, Nadal MH, Eyraud V, Heintz O, Bourillot E (2004) Sens Actuators B 99:58
64. Tang YJ, Fang J, Xu XH, Ji HF, Brown GM, Thundat T (2004) Anal Chem 76:2478
65. Abedinov N, Popov C, Yordanov Z, Ivanov T, Gotszalk T, Grabiec P, Kulisch W, Rangelow IW, Filenko D, Shirshov YJ (2003) Vac Sci Technol B 21:2931
66. Zhou J, Li P, Zhang S, Huang YP, Yang PY, Bao MH, Ruan G (2003) Microelectron Eng 69:37
67. Baselt DR, Fruhberger B, Klaassen E, Cemalovic S, Britton Jr. CL, Patel SV, Mlsna TE, McCorkle D, Warmack B (2003) Sens Actuators B 88:120
68. Fabre A, Finot E, Demoment J, Contreras S (2003) Ultramicroscopy 97:425
69. Zhang YF, Ji HF, Brown GM, Thundat T (2003) Anal Chem 75:4773
70. Zhou J, Li P, Zhang S, Long YC, Zhou F, Huang YP, Yang PY, Bao MH (2003) Sens Actuators B 94:337
71. Lee CY, Lee GB (2003) J Micromech Microeng 13:620
72. Weeks BL, Camarero J, Noy A, Miller AE, Stanker L, De Yoreo JJ (2003) Scanning 25:297
73. Yang YM, Ji HF, Thundat T (2003) J Am Chem Soc 125:1124
74. Gunter RL, Delinger WG, Manygoats K, Kooser A, Porter TL (2003) Sens Actuators A 107:219

75. Gfeller KY, Nugaeva N, Hegner M (2005) Biosens Bioelectron 21:528
76. Alvarez M, Calle A, Tamayo J, Lechuga LM, Abad A, Montoya A (2003) Biosens Bioelectron 18:649
77. Cherian S, Gupta RK, Mullin BC, Thundat T (2003) Biosens Bioelectron 19:411
78. Adams JD, Parrott G, Bauer C, Sant T, Manning L, Jones M, Rogers B, McCorkle D, Ferrell TL (2003) Appl Phys Lett 83:3428
79. Quist F, Tabard-Cossa V, Badia A (2003) J Phys Chem B 107:10691
80. Gunter RL, Zhine R, Delinger WG, Manygoats K, Kooser A, Porter TL (2004) IEEE Sensors J 4:430
81. Alvarez M, Carrascosa LG, Moreno M, Calle A, Zaballos A, Lechuga LM, Martinez C, Tamayo J (2004) Langmuir 20:9663
82. Lee JH, Kim TS, Yoon KH (2004) Appl Phys Lett 84:3187
83. Wu G, Datar RH, Hansen KM, Thundat T, Cote RJ, Majumdar A (2001) Nat Biotechnol 19:856
84. Kim BH, Mader O, Weimar U, Brock R, Kern DP (2003) J Vac Sci Technol B 21:1472
85. Saif MTA, Sager CR, Coyer S (2003) Ann Biomed Eng 31:950
86. Kumar S, Bajpai RP, Bharadwaj LM (2003) IETE Techn Rev 20:361
87. Zhang YF, Venkatachalan SP, Xu H, Xu XH, Joshi P, Ji HF, Schulte M (2004) Biosens Bioelectron 19:1473
88. Pei JH, Tian F, Thundat T (2004) Anal Chem 76:292
89. Khanafer K, Khaled ARA, Vafai K (2004) J Micromech Microeng 14:1328
90. Yue M, Lin H, Dedrick DE, Satyanarayana S, Majumdar A, Bedekar AS, Jenkins JW, Sundaram S (2004) J Microelectromech Syst 13:290
91. Shin S, Paik JK, Lee NE, Park JS, Park HD, Lee J (2005) Ferroelectrics 328:59
92. McFarland AW, Colton JS (2005) J MEMS 14:1375
93. Amirola J, Rodríguez A, Castaner L, Santos JP, Gutierrez J, Horrillo MC (2005) Sens Actuators B 111:247
94. Dutta P, Chapman PJ, Datskos PG, Sepaniak MJ (2005) Anal Chem 77:6601
95. Liu Y, Flood AH, Bonvallett PA, Vignon SA, Northrop BH, Tseng HR, Jeppesen JO, Huang TJ, Brough B, Baller M, Magonov S, Solares SD, Goddard WA, Ho CM, Stoddart JF (2005) J Am Chem Soc 127:9745
96. Tabard-Cossa V, Godin M, Grutter P, Burgués I, Lennox RB (2005) J Phys Chem B 109:17531
97. Tabard-Cossa V, Godin M, Beaulieu LY, Grutter P (2005) Sens Actuators B 107:233
98. Huber F, Hegner M, Gerber C, Güntherodt HJ, Lang HP (2006) Biosens Bioelectron 21:1599
99. Yan XD, Shi XL, Hill K, Ji HF (2006) Anal Sci 22:205
100. Yoo KA, Na KH, Joung SR, Nahm BH, Kang CJ, Kim YS (2006) Japn J Appl Phys Pt 1 45:515
101. Na KH, Kim YS, Kang CJ (2005) Ultramicroscopy 105:223
102. Senesac LR, Dutta P, Datskos PG, Sepaniak MJ (2006) Anal Chim Acta 558:94
103. Mukhopadhyay R, Sumbayev VV, Lorentzen M, Kjems J, Andreasen PA, Besenbacher F (2005) Nano Lett 5:2385
104. Stachowiak JC, Yue M, Castelino K, Chakraborty A, Majumdar A (2006) Langmuir 22:263
105. Castelino K, Kannan B, Majumdar A (2005) Langmuir 21:1956
106. Zhang ZX, Li MQ (2005) Progr Biochem Biophys 32:314
107. Tian F, Hansen KM, Ferrell TL, Thundat T (2005) Anal Chem 77:1601
108. Lee JH, Hwang KS, Park J, Yoon KH, Yoon DS, Kim TS (2005) Biosens Bioelectron 20:2157

109. Ghatnekar-Nilsson S, Lindahl J, Dahlin A, Stjernholm T, Jeppesen S, Hook F, Montelius L (2005) Nanotechnology 16:1512
110. Wig A, Arakawa ET, Passian A, Ferrell TL, Thundat T (2006) Sens Actuators B 114:206
111. Yan XD, Xu XHK, Ji HF (2005) Anal Chem 77:6197
112. Alvarez M, Tamayo J, Plaza JA, Zinoviev K, Dominguez C, Lechuga LM (2006) J Appl Phys 99:024910
113. Khanafer K, Vafai K (2005) Int J Heat Mass Transfer 48:2886
114. Wright YJ, Kar AK, Kim YW, Scholz C, George MA (2005) Sens Actuators B 107:242
115. McFarland AW, Colton JS (2005) J Micromech Microeng 15:1060
116. Rasmussen PA, Grigorov AV, Boisen A (2005) J Micromech Microeng 15:1088
117. Li SQ, Orona L, Li ZM, Cheng ZY (2006) Appl Phys Lett 88:073507
118. Adams JD, Rogers B, Manning L, Hu Z, Thundat T, Cavazos H, Minne SC (2005) Sens Actuators A 121:457
119. Alvarez M, Tamayo J (2005) Sens Actuators B 106:687
120. Tang YJ, Ji HF (2005) Instr Sci Technol 33:131
121. Todorovic DM, Bojicic A (2005) J Phys IV 125:459
122. Sandberg R, Svendsen W, Molhave K, Boisen A (2005) J Micromech Microeng 15:1454
123. Luo C (2005) J Appl Mech – Transactions of the ASME 72:617
124. McFarland AW, Poggi MA, Doyle MJ, Bottomley LA, Colton JS (2005) Appl Phys Lett 87:053505
125. Lochon F, Dufour I, Rebiere D (2005) Sens Actuators B 108:979
126. Dareing DW, Thundat T, Jeon SM, Nicholson M (2005) J Appl Phys 97:084902
127. Dareing DW, Thundat T (2005) J Appl Phys 97:043526
128. Jeon SM, Desikan R, Fang TA, Thundat T (2006) Appl Phys Lett 88:103118
129. Jazar GN (2006) J Vibration Control 12:139
130. Lu P, Lee HP, Lu C, O'Shea SJ (2005) Phys Rev B 72:085405
131. Sheehan PE, Whitman LJ (2005) Nano Lett 5:803
132. Chang MMC, Cuda G, Bunimovich YL, Gaspari M, Heath JR, Hill HD, Mirkin CA, Nijdam AJ, Terracciano R, Thundat T, Ferrari M (2006) Curr Opin Chem Biol 10:11
133. Aeschimann L, Meister A, Akiyama T, Chui BW, Niedermann P, Heinzelmann H, De Rooij NF, Staufer U, Vettiger P (2006) Microelectr Eng 83:1698
134. Yang JL, Despont M, Drechsler U, Hoogenboom BW, Frederix PLTM, Martin S, Engel A, Vettiger P, Hug HJ (2005) Appl Phys Lett 86:134101
135. Yang J, Ono T, Esashi M (2000) Sens Actuators A 82:102